Electrochemistry
The Electrochemical Society of Japan
Received: December 29, 2023
Accepted: January 21, 2024
Published online: January 24, 2024
Issued: April 1, 2024
https://doi.org/10.5796/electrochemistry.23-69165
https://doi.org/10.50892/data.electrochemistry.25045847
Communication
Electrochemistry, **92(4)**, 043008 (2024)

The 69th special feature "Frontiers of Molten Salts and Ionic Liquids"

Electrochemical Intercalation of Cesium into Graphite in Ionic Liquid Electrolyte†

Alisha YADAV,§ Hironobu KOBAYASHI, Takayuki YAMAMOTO,*,§§ and Toshiyuki NOHIRA§§§

Institute of Advanced Energy, Kyoto University, Gokasho, Uji, Kyoto 611-0011, Japan

* *Corresponding author: yamamoto.takayuki.2w@kyoto-u.ac.jp*

ABSTRACT

Graphite is widely used as the negative electrode for alkali-metal ion secondary batteries because of its ability to accommodate various ions between its graphene layers resulting in the formation of graphite intercalation compounds (GICs). In this study, we investigated the intercalation of Cs^+ ions into graphite using an ionic liquid (IL)-based electrolyte, Cs[FTA]–[C_4C_1pyrr][FTA] (FTA = (fluorosulfonyl)(trifluoromethylsulfonyl)amide, C_4C_1pyrr = *N*-butyl-*N*-methylpyrrolidinium). In this electrolyte, the graphite negative electrode imparted an initial reversible capacity of 180 mAh g^{-1} at 298 K. The formation of Cs-GICs was analyzed using an X-ray diffraction technique to reveal the formation of stage-1 CsC_8. The formation potentials of various alkali metal GICs were also compared with respect to the potential of ferrocenium/ferrocene redox couple, revealing that these GICs particularly for stage-1 compounds form in a similar potential range with small differences of 0.2–0.3 V.

Keywords : Cesium-ion Battery, Graphite Intercalation Compounds, Ionic Liquid Electrolyte, Graphite Negative Electrode

1. Introduction

In an effort to decarbonize the transportation sector, there has been a surge in the demand for electric vehicles worldwide.[1–3] Although switching to electric vehicles predominantly reduces the dependence on fossil fuels, it simultaneously presents even more complications particularly exemplified by the depletion of cobalt (Co) resources.[4–6] Co is a key component for the positive electrode materials in Li-ion batteries (LIBs) which are a pioneer for energy storage and conversion systems ranging from portable devices to electric vehicles and stationary energy storage.[7–9] The declining Co resources have led to excessive mining resulting in socio-economic problems.[10,11] Therefore, scientists are focusing on alternative energy storage systems to meet the demands for establishing a carbon-neutral society. Another major issue associated with LIBs is the utilization of highly flammable and volatile organic solvent-based electrolytes, leading to thermal runaway at increasing temperatures.[12,13] In contrast, ionic liquid (IL) electrolytes are nonflammable and less volatile in nature, exhibit high thermal stability, and possess wide electrochemical window, which makes them suitable for constructing safer LIBs as well as next-generation batteries.[14–19]

For metal-ion batteries, graphite is the most commonly used negative electrode material because it is less expensive, environment-friendly, non-toxic, and exhibits high reversible capacity and high conductivity. It is well known that graphite can accommodate various types of ions in between its graphene layers. In the past, several scientists prepared alkali metal GICs using chemical methods.[20–22] In 1926, Fredenhagen and Cadenbach prepared K-, Rb-, and Cs-GICs by mixing alkali metal vapors with graphite in a vacuum tube using a technique typically known as the two-bulb vapor transport technique.[20] In 1958, Asher and Wilson first reported lamellar compounds of Na with graphite having a composition of NaC_{64} examined by X-ray diffraction (XRD) measurements.[21] In 1975, Li-GICs were prepared by Herold using the two-bulb technique.[22]

In the past several decades, the electrochemical intercalation of alkali metal ions into graphite has been investigated extensively for battery applications. The electrochemical intercalation of Li^+ into graphite has been investigated by various groups.[23–25] For the Li-system, graphite exhibits the largest reversible capacity of ~370 mAh g^{-1} (close to the theoretical capacity of 372 mAh g^{-1}) corresponding to the electrochemical formation of LiC_6.[25] Several studies have been conducted for the K-system as well, demonstrating the electrochemical intercalation of K^+ ions into graphite.[26–29] For the K-system a high reversible capacity of 270 mAh g^{-1} (close to the theoretical capacity of 279 mAh g^{-1}) was obtained using 0.8 M KPF_6 in 1 : 1 (v/v) EC : DEC electrolyte. Recently, two research groups including ours, have demonstrated the electrochemical intercalation of Rb^+ into graphite using IL-based electrolytes.[30,31] However, the studies related to the electrochemical intercalation of Cs^+ into graphite are still limited. With the exception of Na^+, all other alkali metal cations intercalate chemically and electrochemically between graphite layers. Therefore, it will be interesting to understand the phenomenon of electrochemical intercalation of Cs^+ into graphite.

In this study, we constructed a Cs-ion battery utilizing Cs[FTA]–[C_4C_1pyrr][FTA] IL as the electrolyte to investigate the electrochemical intercalation mechanism of Cs^+ into graphite and to analyze the possibility of Cs-ion batteries as next-generation batteries. The electrochemical performance as well as the staging

†A part of this paper has been presented in the ECSJ 63rd battery symposium (Presentation #1H09).

§ECSJ Student Member
§§ECSJ Active Member
§§§ECSJ Fellow
A. Yadav orcid.org/0000-0001-7596-3723
T. Yamamoto orcid.org/0000-0003-3553-3272
T. Nohira orcid.org/0000-0002-4053-554X

phenomenon of Cs^+ intercalation into graphite was investigated at room temperature for the first time.

2. Experimental

All electrochemical measurements were conducted using a three-electrode configuration. Graphite composite electrodes were used as both working and counter electrodes due to highly reactive nature of Cs metal and the difficulty of employing Cs metal as the counter electrode. The working electrode was fabricated by mixing commercially available natural graphite powder (SNO-3; SEC Carbon, average particle size: 3 µm) with a sodium carboxymethyl-cellulose (CMC; #2200 Daicel Miraizu Ltd.) binder in a weight ratio of 90 : 10 and the required amount of deionized water to form a homogeneous slurry. The resultant slurry was pasted onto a copper foil using the doctor blade method and dried overnight at 353 K in a vacuum oven. Electrodes with a diameter of 16 mm were then punched out and dried in a vacuum line overnight at 353 K. The slurry for the counter electrode was prepared by mixing natural graphite powder (SNO-10; SEC Carbon, average particle size: 10 µm) with polyvinylidene fluoride (PVdF; Kishida Chemicals Co., Ltd.) binder in a weight ratio of 93 : 7 and the required amount of *N*-methyl-2-pyrrolidone (NMP; FUJIFILM Wako Pure Chemical Co., purity >99 %). The current collector for the counter electrode was aluminum foil. The average loading mass densities of the active materials were approximately 1 mg cm^{-2} and 8 mg cm^{-2} for the working and counter electrodes, respectively. According to our previous reports, FTA^- anions intercalate between graphene layers in IL-related systems,[32,33] and hence graphite was used as a counter electrode for this study. Cs[FTA]–[C_4C_1pyrr][FTA] IL electrolyte with a composition of x(Cs[FTA]) = 0.20, which corresponds to a molar concentration of $C(Cs^+) \approx 0.8$ mol dm^{-3},[18] was prepared by mixing the Cs[FTA] (Provisco CS Ltd., purity >99 %) salt and [C_4C_1pyrr][FTA] IL (Provisco CS Ltd., purity >99 %) in an Ar-filled glove box. Prior to use, the salt and IL were vacuum-dried at 333 K for 1 d. The reference electrode consisted of a Ag wire immersed in [C_3C_1pyrr][FSA] IL (C_3C_1pyrr = *N*-methyl-*N*-propyl-pyrrolidinium, FSA = bis(fluorosulfonyl)amide; Kanto Chemical Co., Ltd.) containing 0.05 mol dm^{-3} of Ag[TfO] (silver trifluoro-methanesulfonate; Sigma-Aldrich), which was separated in a glass tube equipped with a porous glass frit as a liquid junction with the main FTA-based electrolyte. [C_3C_1pyrr][FSA] and Ag[TfO] were vacuum-dried at 333 K for 1 d before use. For M[FTA]–[C_4C_1pyrr][FTA] (M = Li, K, Rb) ILs, charge–discharge measurements were conducted with the same cell configuration. All alkali metal FTA salts were purchased from Provisco CS Ltd. (purity >99 %).

Electrochemical measurements were conducted using a three-electrode cell (SB3A; EC Frontier Co., Ltd.) and a charge–discharge unit (HZ-7000 or HZ-Pro, Meiden Hokuto Corp.). A two-ply glass fiber filter (Whatman, GF/A, diameter = 25 mm, thickness = 260 mm per sheet) was used as the separator. The electrodes and separator were vacuum-impregnated with M[FTA]–[C_4C_1pyrr]-[FTA] (M = alkali metal; x(M[FTA]) = 0.20) electrolyte overnight at 333 K before use. The cell assembly process was conducted in a glove box under dry and deoxygenated argon gas. Taking into consideration the highly reactive nature of Cs-GICs, the cells were sealed in an airtight flask to avoid contact with the air. Galvanostatic charge–discharge measurements of the three-electrode cell were performed at 298 K in a temperature controller (SU-222, ESPEC Corp.). In this study, the capacity (mAh g^{-1}) and current density (mA g^{-1} or C rate) are expressed based on the weight of the active material (graphite) in the working electrode. The potential values are designated with respect to the Ag^+/Ag redox couple. To precisely determine the reaction potentials of graphite in different systems, the potentials were calibrated with respect to the ferrocenium/ferrocene redox couple (Fc^+/Fc). Detailed procedures are provided in the Supporting Information.

Ex-situ X-ray diffraction (XRD) patterns were obtained in Bragg–Brentano geometry using an X-ray diffractometer (Ultima IV, Rigaku Corp.) with Cu-$K\alpha$ radiation (λ = 1.5418 Å) at 40 kV and 40 mA. The samples were transferred to the apparatus in an airtight cell filled with a dry Ar atmosphere.

3. Results and Discussion

Figure 1 shows the charge–discharge curves of the graphite negative electrode for the initial three cycles measured at 298 K using Cs[FTA]–[C_4C_1pyrr][FTA] IL electrolyte. The cell was operated at a constant current rate of 0.5 C (where 1 C corresponds to a current density of 279 mA g^{-1}, assuming the formation of CsC_8) within the potential range of −3.58 to −2.40 V vs. Ag^+/Ag. The total charge and discharge capacities in the 1st cycle are 304 and 185 mAh g^{-1}, respectively, resulting in a coulombic efficiency of 60.9 %. Three distinct potential regions corresponding to the intercalation of Cs^+ are identified for the first charge process: a steep slope (region I) from −2.6 to −3.1 V (vs. Ag^+/Ag), a gentle slope (region II) from −3.1 to −3.3 V, and a long plateau (region III) from −3.4 to −3.58 V. Since a steep slope is not observed for subsequent cycles, the slope region I may correspond to the irreversible decomposition of the electrolyte resulting in solid electrolyte interphase (SEI) formation. This phenomenon is similar to that observed for the Rb-system.[30] The initial charge capacity, excluding the irreversible capacity loss due to the formation of SEI in region I, is approximately 292 mAh g^{-1}, which is still larger by 5 % compared with the theoretical capacity of 279 mAh g^{-1} assuming the formation of CsC_8. Taking the low coulombic efficiency into consideration, irreversible capacity also exists in the regions II and III to a certain extent, which is also attributable to SEI formation. The gentle slope region II and the long plateau region III, which mainly corresponds to the Cs-GIC formation, is also observed for the case of K- and Rb-GICs. However, considering the two-phase coexistence state (e.g. stage 1 and stage 2 GICs), the plateau region appears more sloping than expected, and the large overpotentials are observed for Cs-GICs. These phenomena can be attributed to the cell configuration. Since the reference electrode used in the present study consists of a Ag wire immersed in the Ag[TfO]–[C_3C_1pyrr][FSA] reference electrolyte and is separated by a porous glass frit from the main electrolyte, the distance between the working and reference electrodes is longer than that in the two-electrode coin cell, leading to a higher bulk electrolyte impedance. Similar behavior has been observed in our previous study on Rb intercalation into graphite.[30] Moreover, for graphite negative electrodes in K-system, we previously confirmed smaller polarizations in two-electrode coin cells using porous composite

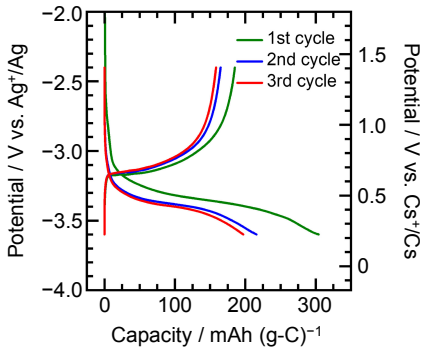

Figure 1. Charge–discharge curves of a graphite negative electrode in Cs[FTA]–[C_4C_1pyrr][FTA] (x(Cs[FTA]) = 0.20) IL electrolyte at 0.5 C current rate and 298 K.

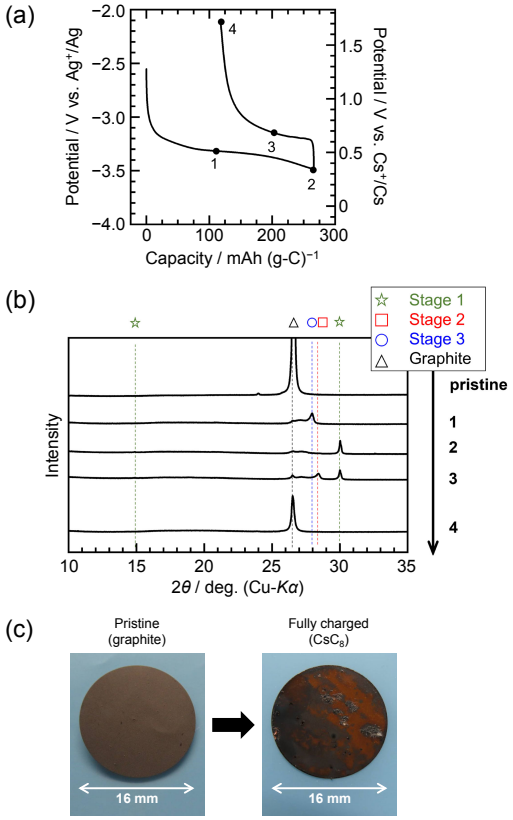

Figure 2. (a) Charge–discharge curves of a graphite negative electrode in Cs[FTA]–[C_4C_1pyrr][FTA] (x(Cs[FTA]) = 0.20) IL electrolyte at 298 K. Current rate: 0.1 C after cycling at 0.5 C for 3 cycles. (b) Ex-situ XRD patterns of graphite electrodes at different charge–discharge states; numbering provided in the figure corresponds to points plotted in Fig. 2a. (c) Change in the whole surface image of graphite electrode during charge process from pristine (graphite) to fully charged (CsC_8).

electrodes,[33] which excludes the dominant contribution of porous-type electrodes to the sloping behavior in three-electrode configuration. The discharge capacity gradually decreases with subsequent cycling, reaching 158 mAh g^{-1} in the 3rd cycle. On the other hand, the irreversible capacity is significantly reduced, and the improved coulombic efficiency of 80.3 % is observed in the 3rd cycle.

To elucidate the phase evolution behavior of graphite upon Cs^+ intercalation/deintercalation, ex-situ XRD measurements were performed on graphite negative electrodes at different states of charge (SOCs). Figure 2a shows the representative charge–discharge curves at 0.1 C. The potential axis with respect to Cs^+/Cs potential is also provided as a reference based on our previous report.[18] To ensure that the SEI formation is complete, the cell was subjected to the aging process for one cycle at 0.5 C and then followed by one cycle at 0.1 C current rate between a voltage range of −3.50 to −2.10 V. For the preparation of the electrodes at different SOCs, the cells for points 1–3 were subjected to the charge–discharge conditions similar to the cell in Fig. 2a. In contrast, the cell for point 4 was subjected to three cycles at 0.5 C between −3.70 to −2.10 V and then one cycle at 0.1 C between −3.58 to −2.10 V.

Figure 2b shows the ex-situ XRD patterns of the graphite negative electrodes for different SOCs. The points in Fig. 2a correspond to the points mentioned in Fig. 2b. Initially, only the graphite peak (26.58°) is observed for the pristine graphite electrode. Upon charging to point 1 (105 mAh g^{-1}), a broad peak at 26.5–27.5° and a sharp peak at 28.0° are observed. The broad peak can be attributed to the presence of graphite and multiple high-stage Cs-GICs. The sharp peak is considered to correspond to stage-3 Cs-GIC. At the fully charged state, at point 2 (266 mAh g^{-1}), Cs-GIC peaks assigned to stage 1 are obtained. However, two faint diffraction peaks are simultaneously observed at 26.5° and 27.5°, which can be attributed to the unreacted graphite and dilute stages, respectively. On the other hand, during discharge, XRD peaks corresponding to stage 2 and stage 1 Cs-GICs are also observed at point 3 (205 mAh g^{-1}). A peak is also observed at 26.5°, which may be ascribed to unreacted graphite in the electrode. Only the graphite peak is observed in the fully discharged state at point 4 (118 mAh g^{-1}). According to the previous reports,[34–38] the Cs-GIC compositions of stage 3, stage 2, and stage 1 are CsC_{36}, CsC_{24}, and CsC_8, respectively. Figure 2c also confirms the formation of CsC_8 at the end of charge process with the change in the color of the electrode to dark brown. The obtained discharge capacity of 148 mAh g^{-1} in Fig. 2b is much lower than the theoretical capacity (279 mAh g^{-1}). This is consistent with the appearance of the fully charged electrodes (Fig. 2c), where some parts of the electrode surface remain unreacted. Moreover, a large irreversible capacity of 118 mAh g^{-1} is observed, indicating the considerable SEI formation during the charge process. Considering the uneven formation of Cs-GICs, thick and non-uniform SEI formation may occur on the surface of graphite negative electrode, hindering the full utilization of active material.

The interlayer distance (d_i) of stage 1 CsC_8 is calculated to be 5.94 Å, which is a factor of ∼1.8 higher than that between the graphene layers of graphite before intercalation (d_0 = 3.35 Å). It is worth noting that the intensity of the graphite peak at point 4 has decreased compared to the pristine graphite state. The intercalation and deintercalation of large Cs^+ ions into/from the graphite electrode probably result in the decrease in crystallinity of graphite, likely arising from the variation in the interlayer distance of graphite, which was also observed in the Rb-system.[30] The I_c and d_i values calculated for the Cs-GICs are listed in Table 1. The obtained d_i values lie within the range of 5.94–6.07 Å, which is almost consistent with those in the previous studies on the chemical synthesis of Cs-GICs.[34–38] The I_c and d_i values from the present and previous studies are summarized in Table 2.

To ascertain the long-term cycling stability of graphite negative electrodes for a Cs-system, a charge–discharge test was conducted at 298 K, as shown in Fig. 3. Cycling tests were performed at a relatively high current rate of 1 C for 100 cycles in the potential range of −3.69 to −2.10 V vs. Ag^+/Ag. The initial charge and discharge capacities are 151 and 126 mAh g^{-1}, resulting in a coulombic efficiency of 83.9 %. The charge–discharge profiles of the 1st, 5th, 30th, 50th, and 100th cycles do not overlap each other with continuous increase in polarization (Fig. 3a). Unlike the Rb-system,[30] the capacity for the Cs-system decreases rapidly during the initial cycles and does not recover even after a few cycles (Fig. 3b). At last, the discharge capacity decreases to 52.9 mAh g^{-1} after 50 cycles. This behavior can possibly be attributed to the severe volume change between pristine graphite and CsC_8, affecting the instability of the SEI.

Finally, the formation phenomenon of the GICs were compared among IL electrolytes for different alkali metals using the three-electrode cells composed of graphite negative and positive electrodes and an Ag^+/Ag reference electrode. The potentials were calibrated with respect to that of the Fc^+/Fc redox couple. Figure 4

Table 1. The obtained values of repeated distance (I_c) and the distance between the intercalated layers (d_i) for stage n Cs-GIC samples prepared at a current rate of 0.1 C and 298 K.

Compound	Stage index (n)	I_c/Å		d_i/Å
		Intercalation	Deintercalation	
CsC_8	1	5.94	5.94	5.94
CsC_{24}	2	—	9.40–9.42	6.05–6.07
CsC_{36}	3	12.76	—	6.06

Table 2. Summary of the present and representative previous studies on Cs-GICs.

Year	Authors	Stage index (n) or Compound	I_c/Å	d_i/Å	Remarks	Ref.
2023	Yadav et al.	Stage 1 (CsC_8)	~5.94	~5.94	X-ray diffraction	This study
		Stage 2 (CsC_{24})	~9.41	~6.06		
		Stage 3 (CsC_{36})	12.76	~6.06		
1978	Mizutani et al.	Stage 1 (CsC_8) Stage 2 (CsC_{24}) Stage 3 (CsC_{36})	—	5.94	X-ray diffraction	34
1979	Leung et al.	Stage 1 (CsC_8)	5.95	~5.95	X-ray diffraction (Mo$K\alpha$)	35
		Stage 2 (CsC_{24})	9.36	~6.01		
1981	Sano et al.	Stage 1 (CsC_8)	5.96	5.96	X-ray diffraction	36
1981	Wada et al.	Stage 1 (CsC_8)	~5.943	~5.943	X-ray diffraction	37
1981	Leung et al.	Stage 1	5.95	5.95	X-ray diffraction	38
		Stage 2	9.37	6.02		

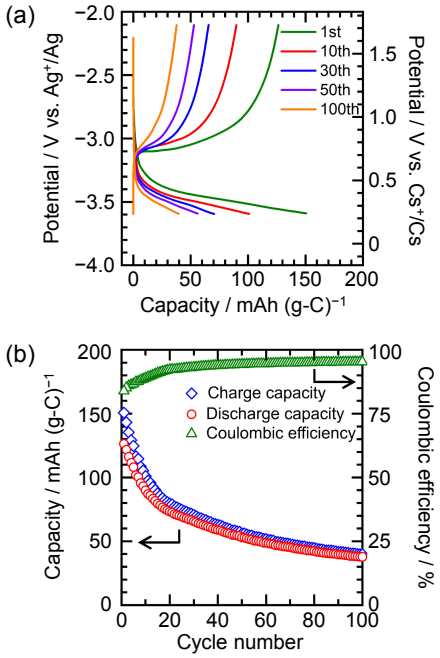

Figure 3. (a) Charge–discharge curves and (b) cycling properties of a graphite negative electrode in Cs[FTA]–[C_4C_1pyrr][FTA] (x(Cs[FTA]) = 0.20) IL electrolyte at 1 C current rate and 298 K.

shows the charge–discharge curves of a graphite negative electrode using a three-electrode cell in M[FTA]–[C_4C_1pyrr][FTA] (M = Li, K, Rb, and Cs) IL electrolyte at certain current rates and 298 K. Prior to the measurement, the cells were pre-cycled within the certain conditions. The detailed results of the Fc^+/Fc redox potential measurements are provided in Supporting Information. Charge–discharge rates were set at 0.1 C (= 37.2 mA g^{-1}) for Li-system, 0.1 C (= 27.9 mA g^{-1}) for K-system, 0.05 C (= 13.95 mA g^{-1}) for Rb-system, and 0.1 C (= 27.9 mA g^{-1}) for Cs-system. According to the charge–discharge curves of the K-, Rb-, and Cs-systems, the long plateaus observed in the most negative potential regions, which is characteristic of the formation of stage-1 GICs, are sloping, which induces the larger potential deviations between the charge and discharge processes. As mentioned above (See Fig. 1), one of the reasons for the large overpotentials is the cell configuration because charge–discharge curves of similar graphite composite electrodes obtained by two-electrode coin-type cell with K metal counter electrode showed much smaller overpotentials for K-system.[33] Particularly for the Cs-system, the color of the electrode showed the presence of some unreacted graphite. This suggests the formation of thick and non-uniform SEI on the surface of electrode, presumably limiting the intercalation of Cs^+ ions. We chose the cut-off potential of −3.21 V (vs. Fc^+/Fc) for the Cs-system, which is higher than the Cs deposition potential of −3.45 V. This is because, as described above, the SEI formation during the first cycle is quite high in the Cs-system, leading to low coulombic efficiency and severe deterioration of the graphite negative electrodes. Namely we considered that cell operation with a higher cut-off potential would

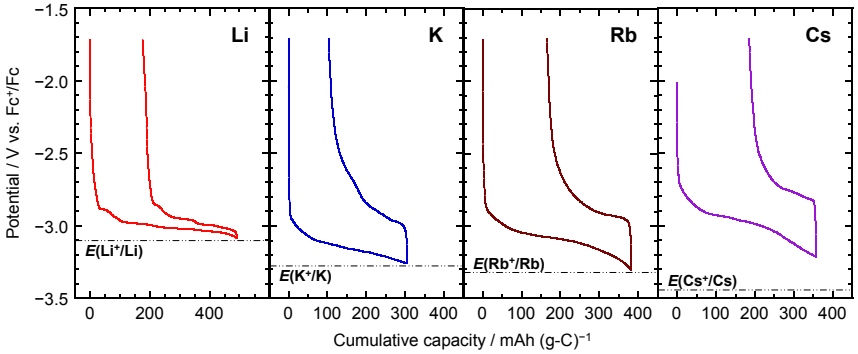

Figure 4. Comparison of charge–discharge curves of a graphite negative electrode in a three-electrode cell using M[FTA]–[C_4C_1pyrr][FTA] (M = Li, K, Rb,[30] Cs) IL electrolyte at the specified current rate and 298 K. The potential was calibrated with respect to the redox couple of Fc^+/Fc. The current rate of 1 C corresponds to 372 mA g^{-1} for Li-system and 279 mA g^{-1} for K-, Rb-, and Cs-systems.

help to mitigate the negative effect of unnecessarily thick SEI formation and to obtain higher reversible capacities.

The long plateaus corresponding to the formation of stage-1 GICs in the charge process lie within a similar potential range with small differences of 0.2–0.3 V, i.e., −3.0 V (vs. Fc^+/Fc) for Li, −3.15 V for K, −3.1 V for Rb, and −3.0 V for Cs. Although the potential polarizations are large for K-, Rb-, and Cs-systems, the equilibrium potential between stage-1 and stage-2 GIC in each system is considered to positively shift in the order of K < Rb < Cs because both the charging and discharging curves of these three systems move towards higher potentials in this order. In our previous study, the charge–discharge behavior of a graphite negative electrode was investigated using M[FSA]–[C_3C_1pyrr][FSA] (M = Li, Na, K) IL electrolytes, which revealed that the virtual onset potential of M-GIC formation is considered to shift negatively from Li to K,[19] which is consistent with the case of FTA-based ILs used in the present study. Thus, it is concluded that the formation potential of alkali metal-GICs, especially for the stage-1 compounds, is most negative for the K-system, and it increases towards the Li- or Cs-system. Since the formation mechanism of alkali metal GICs is similar among K-, Rb-, and Cs-systems, the upshift in the Cs-GIC formation potential can be simply explained by the GIC properties. According to a previous report, structural deformation energy of graphene layers and the binding energy in the presence of intercalants are involved with phase transition from graphite to GICs.[39] There may be favorable interactions of graphene layers with Cs^+ ions having lower charge densities, which overcomes the structural deformation energy of large-sized Cs^+ ions.

4. Conclusions

In this study, the charge–discharge behavior of graphite negative electrodes for Cs-ion batteries was investigated using the Cs[FTA]–[C_4C_1pyrr][FTA] electrolyte at 298 K. The initial charge and discharge capacities of 304 and 185 mAh g^{-1} were achieved at a rate of 0.5 C, entailing the formation of stage-1 Cs-GIC (CsC_8) with $d_i = 5.94$ Å confirmed by ex-situ XRD measurements. Finally, we compared the electrochemical performance of various alkali metals in graphite and revealed that the formation potential of all alkali metal GICs lies in a similar potential region with a small difference of 0.2–0.3 V.

Acknowledgments

This study was partly supported by JSPS KAKENHI grants (JP18K14320 and JP21K14718), the Research Foundation for the Electrotechnology of Chubu, the Kyoto University Foundation, the Murata Science and Education Foundation, and ISHIZUE 2023 of Kyoto University. We thank SEC Carbon, Ltd. for supplying the graphite powders. We also thank Daicel Miraizu Ltd. for supplying the CMC powder.

CRediT Authorship Contribution Statement

Alisha Yadav: Data curation (Equal), Investigation (Equal), Methodology (Equal), Validation (Equal), Writing – original draft (Lead)
Hironobu Kobayashi: Data curation (Equal), Investigation (Lead), Methodology (Equal), Validation (Equal), Writing – review & editing (Supporting)
Takayuki Yamamoto: Conceptualization (Equal), Data curation (Equal), Funding acquisition (Lead), Methodology (Equal), Supervision (Equal), Validation (Equal), Writing – review & editing (Equal)
Toshiyuki Nohira: Conceptualization (Equal), Methodology (Equal), Supervision (Equal), Validation (Equal), Writing – review & editing (Equal)

Data Availability Statement

The data that support the findings of this study are openly available under the terms of the designated Creative Commons License in J-STAGE Data listed in D1 of References.

Conflict of Interest

The authors declare that they have no known competing financial interests.

Funding

Japan Society for the Promotion of Science: JP18K14320, JP21K14718
The Research Foundation for the Electrotechnology of Chubu
The Kyoto University Foundation
The Murata Science and Education Foundation
ISHIZUE 2023 of Kyoto University

References

D1. A. Yadav, H. Kobayashi, T. Yamamoto, and T. Nohira, *J-STAGE Data*, https://doi.org/10.50892/data.electrochemistry.25045847, (2024).
1. Z. Li, A. Khajepour, and J. Song, *Energy*, **182**, 824 (2019).
2. Z. P. Cano, D. Banham, S. Ye, A. Hintennach, J. Lu, M. Fowler, and Z. Chen, *Nat. Energy*, **3**, 279 (2018).
3. IEA, *Global EV Outlook 2023*, IEA (2023). https://www.iea.org/reports/global-ev-outlook-2023.
4. J. Deng, C. Bae, A. Denlinger, and T. Miller, *Joule*, **4**, 511 (2020).
5. B. E. Lebrouhi, Y. Khattari, B. Lamrani, M. Maaroufi, Y. Zeraouli, and T. Kousksou, *J. Energy Storage*, **44**, 103273 (2021).
6. C. Xu, Q. Dai, L. Gaines, M. Hu, A. Tukker, and B. Steubing, *Commun. Mater.*, **1**, 99 (2020).
7. K. Mizushima, P. C. Jones, P. J. Wiseman, and J. B. Goodenough, *Mater. Res. Bull.*, **15**, 783 (1980).
8. K. Ozawa, *Solid State Ionics*, **69**, 212 (1994).
9. J. B. Goodenough and K. S. Park, *J. Am. Chem. Soc.*, **135**, 1167 (2013).
10. A. L. Gulley, *Resour. Policy*, **79**, 103007 (2022).
11. M. van der Meide, C. Harpprecht, S. Northey, Y. Yang, and B. Steubing, *J. Ind. Ecol.*, **26**, 1631 (2022).
12. T. Tsujikawa, K. Yabuta, T. Matsushita, T. Matsushima, K. Hayashi, and M. Arakawa, *J. Power Sources*, **189**, 429 (2009).
13. C. Arbizzani, G. Gabrielli, and M. Mastragostino, *J. Power Sources*, **196**, 4801 (2011).
14. H. Matsumoto, N. Terasawa, T. Umecky, S. Tsuzuki, H. Sakaebe, K. Asaka, and K. Tatsumi, *Chem. Lett.*, **37**, 1020 (2008).
15. K. Kubota, T. Nohira, R. Hagiwara, and H. Matsumoto, *Chem. Lett.*, **39**, 1303 (2010).
16. I. Hasa, S. Passerini, and J. Hassoun, *J. Power Sources*, **303**, 203 (2016).
17. T. Yamamoto, K. Matsumoto, R. Hagiwara, and T. Nohira, *J. Phys. Chem. C*, **121**, 18450 (2017).
18. T. Yamamoto, S. Nishijima, and T. Nohira, *J. Phys. Chem. B*, **124**, 8380 (2020).
19. T. Yamamoto, A. Yadav, and T. Nohira, *J. Electrochem. Soc.*, **169**, 050507 (2022).
20. K. Fredenhagen and G. Cadenbach, *Z. Anorg. Allg. Chem.*, **158**, 249 (1926).
21. R. C. Asher and S. A. Wilson, *Nature*, **181**, 409 (1958).
22. D. Guerard and A. Herold, *Carbon*, **13**, 337 (1975).
23. R. Yazami and P. Touzain, *J. Power Sources*, **9**, 365 (1983).
24. R. Fong, U. Von Sacken, and J. R. Dahn, *J. Electrochem. Soc.*, **137**, 2009 (1990).
25. T. Ohzuku, Y. Iwakoshi, and K. Sawai, *J. Electrochem. Soc.*, **140**, 2490 (1993).
26. Z. Jian, W. Luo, and X. Ji, *J. Am. Chem. Soc.*, **137**, 11566 (2015).
27. S. Komaba, T. Hasegawa, M. Dahbi, and K. Kubota, *Electrochem. Commun.*, **60**, 172 (2015).
28. K. Beltrop, S. Beuker, A. Heckmann, M. Winter, and T. Placke, *Energy Environ. Sci.*, **10**, 2090 (2017).
29. L. Fan, R. Ma, Q. Zhang, X. Jia, and B. Lu, *Angew. Chem.*, **131**, 10610 (2019).
30. A. Yadav, H. Kobayashi, T. Yamamoto, and T. Nohira, *Electrochemistry*, **91**, 017002 (2023).
31. D. Igarashi, R. Tatara, R. Fujimoto, T. Hosaka, and S. Komaba, *Chem. Sci.*, **14**, 11056 (2023).
32. T. Nikaido, A. Yadav, T. Yamamoto, and T. Nohira, *J. Electrochem. Soc.*, **170**, 020526 (2023).
33. A. Yadav, H. Kobayashi, T. Nikaido, T. Yamamoto, and T. Nohira, *J. Power Sources*, **585**, 233628 (2023).
34. U. Mizutani, T. Kondow, and T. B. Massalski, *Phys. Rev. B*, **17**, 3165 (1978).
35. S. Y. Leung, C. Underhill, G. Dresselhaus, T. Krapchev, R. Ogilvie, and M. S. Dresselhaus, *Solid State Commun.*, **32**, 635 (1979).
36. M. Sano, N. Sato, H. Inokuchi, and S. Tamura, *Bull. Chem. Soc. Jpn.*, **54**, 2610 (1981).
37. N. Wada, *Phys. Rev. B*, **24**, 1065 (1981).
38. S. Y. Leung, M. S. Dresselhaus, C. Underhill, T. Krapchev, G. Dresselhaus, and B. J. Wuensch, *Phys. Rev. B*, **24**, 3505 (1981).
39. O. Lenchuk, P. Adelhelm, and D. Mollenhauer, *Phys. Chem. Chem. Phys.*, **21**, 19378 (2019).